

Trajectory dependent entanglement transition in a free fermion chain – from extended criticality to area law

O. Alberton,¹ M. Buchhold,¹ and S. Diehl¹

¹*Institut für Theoretische Physik, Universität zu Köln, D-50937 Cologne, Germany*

(Dated: December 22, 2024)

We analyze the quantum trajectory dynamics of free fermions subject to non-unitary dephasing processes. The non-unitary evolution can either be motivated by a "monitored" open system dynamics, or by a continuous non-unitary circuit evolution, each leading to a different set of trajectories. Despite each set yielding the same trajectory averaged density matrix, governed by one Lindblad quantum master equation, we demonstrate significant structural differences in their trajectory statistics. For weak dephasing, the difference remains marginal and we observe subextensive entanglement growth, reminiscent of a critical phase with an emergent conformal invariance. For strong dephasing, however, the dynamics either favors a transition into a quantum Zeno-like area-law regime, or extends the logarithmic growth to arbitrarily strong dephasing rates. This shows that the choice of the trajectory evolution can be essential for the existence of entanglement transitions, and enables the study of unconventional entanglement dynamics in an elementary, physically realistic model for weak continuous measurements.

Introduction. – Fingerprints of the competition between unitary and non-unitary dynamics are found in almost all aspects of modern quantum science. The spectrum ranges from radiative decay in driven two-level systems [1, 2] to dephasing of trapped ions and cold atoms due to laser noise [3] or phonon-induced dissipation in electronic devices and color centers [4, 5]. Non-unitary processes crucially affect quantum dynamics from single particles to the many-body realm.

One fascinating example are phase transitions in the entanglement entropy, which have been discovered in unitary circuit dynamics subject to local projective measurements [7–12]. Focussing on the entanglement properties of individual measurement trajectories $|\psi(\xi)\rangle$, where $\xi(t)$ is a realization of temporal randomness encountered in quantum mechanical measurements, a transition from an entangling evolution obeying a volume-law to a disentangled evolution governed by an area-law as a function of the measurement rate has been identified [13–19]. A characteristic trait of these transitions is that they manifest themselves in *state-dependent* observables $\hat{O}(\rho(\xi))$, with $\rho(\xi) = |\psi(\xi)\rangle\langle\psi(\xi)|$. For example, for the entanglement entropy of a subsystem A, $\hat{O}(\rho(\xi)) = -\log \rho_A(\xi)$, where $\rho_A(\xi)$ is the reduced density matrix on A – a highly nonlinear function of the state $\rho(\xi)$. Such entanglement transitions have been reported in a plethora of setups, including non-unitary circuit models and chains of interacting bosons subject to continuous measurements [20–24].

Here we focus on one of the most elementary models for the competition between unitary and non-unitary dynamics, free fermions on a periodic chain, subject to coherent hopping and local, temporally random, and particle number conserving dephasing dynamics [25–28]. This model can be simulated efficiently [26], allowing to investigate large system sizes, similarly to the case of random Clifford circuits. In addition, it is natural in terms of physical implementations: this scenario arises, e.g., for ultracold fermions in optical lattices, which experience incoherent light scattering [25, 29], or in Rydberg atom arrays subject to phase noise in the driving laser [30, 31]. From a measurement theory point of view, the non-unitary de-

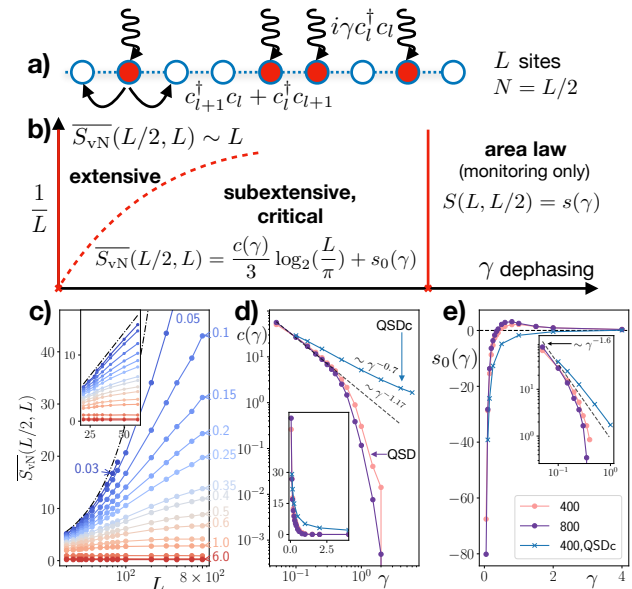


Figure 1. (a) Free fermions hopping on a chain of length L subject to continuous monitoring with dimensionless rate γ . (b) Schematic "phase diagram" showing the different regimes of entanglement scaling with L . (c) At small monitoring rate, a subextensive growth of the entropy $\sim \log(L)$ at sufficiently large L is reminiscent of a critical, conformally invariant phase. For small γ, L , extensive growth $\sim L$ is observed (inset), approaching a volume law as $\gamma \rightarrow 0$. (d,e) The effective central charge and residual entropy obtained by fitting the data to Eq. (4). Depending on the trajectory evolution, the logarithmic growth is either cut off at a critical monitoring rate and passes into an area-law regime, or persists up to arbitrarily large γ . The insets show the same data on a linear (d) and logarithmic (e) scale [6].

phasing evolution results from a continuous, weak measurement of the local fermion particle number, caused for instance by weak interactions with a monitored photon bath [32–35].

As a main result, we find that the way monitoring is performed is essential for the qualitative properties of entanglement entropy dynamics – in fact, this goes as far as detecting

or not a phase transition in the trajectory dynamics at finite measurement rate. Central to this finding is whether probability is conserved exactly in the trajectory evolution, or only on average. While exact probability conservation is automatic in unitary dynamics, it may or may not be realized for non-unitary protocols – even though the average conservation is sufficient to guarantee a consistent open system quantum dynamics. In particular, all considered protocols collapse onto the same Lindblad quantum master equation (QME). The difference surfaces however once state dependent observables are considered: Amongst the trajectory evolutions considered here, only non-unitary protocols with exact probability conservation exhibit an entanglement phase transition.

The entanglement phase diagram is displayed in Fig. 1. As a function of γ/J , where γ is the dephasing rate and J describes the coherent hopping of fermions used to set the units from here on ($J = 1$), three qualitatively different behaviors of the entanglement entropy can be realized: A volume law $\sim L$, a subextensive scaling $\sim \log L$, and an area law $\sim L^0$. The intriguing subextensive behavior reminiscent of a conformal field theory (CFT) has also been observed very recently in a related free fermion model including spatio-temporal randomness [24], and in measurement-only protocols [36]. As in [24], we find that the volume law realized at $\gamma = 0$ is unstable against infinitesimal dephasing $\gamma > 0$. The opposite limit $\gamma^{-1} = 0$ of local dephasing dynamics without entangling operations is trivially characterized by an area law. Its stability against small perturbations is more subtle: it only ensues when probability is conserved exactly. In this case, a phase transition from a critical logarithmic CFT scaling behavior with γ dependent central charge, to an area law at a finite γ_c (cf. Fig. 1) appears, similarly to [36], and accompanied by a sudden drop of the central charge to zero. On the other hand, this transition is absent, or pushed to infinity, for a non-unitary protocol with average probability conservation.

Trajectory evolution. – We consider free fermions on a half-filled periodic chain of length L , which is described by the nearest-neighbor hopping Hamiltonian $H = \sum_l c_{l+1}^\dagger c_l + c_l^\dagger c_{l+1}$ with fermionic creation and annihilation operators c_l^\dagger, c_l . Due to the weak measurements of the fermion density the time-evolution of a fermion pure state $|\psi(\{\xi_{l,t}\})\rangle$ follows a stochastic trajectory, determined by a set of noise increments $\{\xi_{l,t}\}$. They describe the random interactions of the local fermion density with a (monitoring) environment $\sim i\xi_{l,t}n_l$.

The three types of trajectory dynamics we consider are: (i) the quantum state diffusion (QSD), which describes fermions interacting with a bath of photons, which are continuously monitored via homodyne detection [37, 38], (ii) the quantum jump evolution (QJ), corresponding to the same bath but photons scattering off fermions are counted directly [34, 35, 39] and (iii) a so-called "raw" quantum state diffusion [33, 38, 40], mimicking a non-unitary circuit evolution (QSDc).

The wave functions in the QSD and the QSDc trajectories

follow the evolution equation

$$d|\psi(\{\xi_{l,t}\})\rangle = \left[-iHdt + \sum_l \left(\frac{\gamma}{2} \hat{M}_{l,t}^2 dt + \xi_{l,t} \hat{M}_{l,t} \right) \right] |\psi(\{\xi_{l,t}\})\rangle, \quad (1)$$

where $\hat{M}_{l,t} = n_l - \sigma \langle n_l \rangle_t$ and $\sigma = 1$ ($\sigma = 0$) for the QSD (QSDc) case. The real-valued Gaussian noise $\xi_{l,t}$ has zero mean $\xi_{l,t} = 0$ and autocorrelations $\xi_{l,t} \xi_{m,t'} = \gamma dt \delta_{l,m} \delta(t - t')$.

In the quantum jump trajectories, the evolution equation is

$$d|\psi(\{\xi_{l,t}\})\rangle = \left[-iHdt + \sum_l \xi_{l,t} \left(\frac{n_l}{\sqrt{\langle n_l \rangle_t}} - 1 \right) \right] |\psi(\{\xi_{l,t}\})\rangle, \quad (2)$$

for a state with conserved total particle number. For QJ the noise is defined via $\xi_{l,t}^2 = \xi_{l,t}$ and $\overline{\xi_{l,t}} = \gamma dt \langle n_l \rangle_t$, i.e. the $\xi_{l,t}$ are independently distributed according to $P(\xi_{l,t}) = \delta_{\xi_{l,t}, 1} \overline{\xi_{l,t}} + \delta_{\xi_{l,t}, 0} (1 - \overline{\xi_{l,t}})$.

For each trajectory evolution, the statistical average over the noise distribution $P(\{\xi_{l,t}\})$ defines the density matrix

$$\overline{|\psi(\{\xi_{l,t}\})\rangle \langle \psi(\{\xi_{l,t}\})|} \equiv \int \mathcal{D}(\xi_{l,t}) P(\{\xi_{l,t}\}) |\psi(\{\xi_{l,t}\})\rangle \langle \psi(\{\xi_{l,t}\})| = \rho_t.$$

For all three types of trajectories the density matrix evolution is given by the deterministic QME with Markovian dephasing

$$\partial_t \rho = -i[H, \rho] + \gamma \sum_l (2n_l \rho n_l - \{n_l^2, \rho\}). \quad (3)$$

Time-evolved correlations and entanglement. – The evolution equations, Eqs. (1), (2), are quadratic in the fermion operators and any initial Gaussian state $|\psi_0\rangle$ thus remains Gaussian under time evolution. Hence, the state $|\psi_t\rangle$ at time t may be parametrized as

$$|\psi_t\rangle = \prod_{l=1}^N \left(\sum_{j=1}^L u_{j,l}(t) c_j^\dagger \right) |0\rangle, \text{ with } \sum_{j=1}^L u_{j,m}^*(t) u_{j,l}(t) = \alpha_{l,t} \delta_{l,m},$$

where N is the number of fermions and $\prod_l \alpha_{l,t} = \langle \psi_t | \psi_t \rangle$ is the norm of the state ($\alpha_{l,t} = 1$ for QSD and QJ). The correlation matrix $D(t, t')$ defined by

$$D_{l,j}(t, t') = \sum_{m=1}^N u_{j,m}(t') u_{l,m}^*(t) \prod_{l=1}^N \frac{1}{\alpha_{l,t}} = \langle c_{l,t}^\dagger c_{j,t'} \rangle$$

contains all information on the fermion correlation functions. The Gaussian structure of the state enables efficient numerical simulation of Eqs. (1), (2), which is outlined in Refs. [26, 40].

For a chain of length L , the von Neumann entanglement entropy $S_{\text{vN}}(l, L)$ for a subsystem $A = [m_1, m_2]$ of length $l = |m_1 - m_2|$ is obtained from the eigenvalues $\{\lambda_j^{(A)}\}$ of the reduced equal-time correlation matrix $D^{(A)}(t, t) = D_{i=m_1, \dots, m_2, j=m_1, \dots, m_2}(t, t)$ on A via [41, 42]

$$S_{\text{vN}}(l, L) = - \sum_{j=1}^l \lambda_j^{(A)} \log_2 \lambda_j^{(A)} + (1 - \lambda_j^{(A)}) \log_2 (1 - \lambda_j^{(A)}).$$

The mutual information $\mathcal{I}(l_A, l_B)$ between two disjoint subsystems $A = [m_1, m_2]$, $B = [m_3, m_4]$ of length l_A, l_B is a useful indicator for the location of the entanglement transition [18]. It is obtained via $\mathcal{I}(l_A, l_B) = S_{\text{vN}}(l_A, L) + S_{\text{vN}}(l_B, L) - S_{\text{vN}}(A \cup B, L)$.

In addition to the entanglement entropy and mutual information, we consider the square of the correlation functions

$$C(l, \tau) \equiv |D_{l+j,j}(t + \tau, t)|^2 = \langle n_{l+j,t+\tau} \rangle \langle n_{j,t} \rangle - \langle n_{l+j,t+\tau} n_{j,t} \rangle,$$

which is the Fock (exchange) contribution to the density-density correlation in a Gaussian state.

In what follows we initialize the system in a short range correlated Néel state $|\psi_0\rangle = |010101\dots01\rangle$, and evolve the different types of trajectories according Eqs. (1), (2). The entanglement entropy, mutual information and correlation functions are computed for each individual trajectory after the evolution has reached a steady state, $\gamma t \gg 1$ [40]. We denote the statistical average of an observable O by \overline{O} . For nonlinear functions $f(D)$ of the correlation matrix, $\overline{f(D)} \neq f(\overline{D})$ in general and therefore $S_{\text{vN}}(l, L)$, $\mathcal{I}(l_A, l_B)$, $C(l, \tau)$ cannot be obtained from the trajectory averaged correlation matrix \overline{D} or from the QME (3). Hence, different trajectory evolutions may yield different results when the entanglement entropy or other objects which are non-linear in D are considered.

Entropy growth and phase diagram. – For a bipartition of the chain into two equal subsystems, the steady-state entanglement entropy $S_{\text{vN}}(L/2, L)$ shows three different dependences on the chain length L and the monitoring rate γ , as illustrated in Fig. 1(c) for the case of QSD evolution and in [40] for QJ evolution. For the coherent time evolution at $\gamma = 0$, an initial Néel state develops an extensive entanglement entropy converging to a volume law [42]. This behavior transcends to slow but non-zero monitoring, where one still observes an extensive entanglement growth $S_{\text{vN}}(L/2, L) \sim L$ for $L < L_c(\gamma)$ smaller than a γ -dependent cutoff length.

Around $L \sim L_c(\gamma)$, the entanglement entropy smoothly crosses over from an extensive to a subextensive growth $S(L) \sim \log L$. For $0 < \gamma \leq 0.25$, this crossover is observed for any sufficiently large system with size $L > L_c(\gamma)$. For $\gamma \rightarrow 0$, $L_c(\gamma) \rightarrow \infty$ diverges, following roughly a stretched exponential $L_c(\gamma) \sim \exp[-(\gamma_0/\gamma)^\alpha]$ with $\alpha \approx 0.6$ [43]. The asymptotic behavior of the entanglement entropy for $L \rightarrow \infty$ is thus always logarithmic for small γ . In any finite-size system, however, an extensive entanglement entropy is observed once $L_c(\gamma)$ exceeds the system size, e.g., for $\gamma < 0.15$ system sizes $L < L_c(0.15) \approx 35$ appear like having volume law, see the inset of Fig. 1(c).

Logarithmic growth of the entanglement entropy is characteristic for $(1+1)$ -dimensional conformal field theories (CFTs) [44, 45]. Here, the logarithmic dependence of the entanglement entropy is similar to a CFT with periodic boundaries

$$\overline{S_{\text{vN}}}(l, L) = \frac{c(\gamma)}{3} \log_2 \left[\frac{L}{\pi} \sin \left(\frac{\pi l}{L} \right) \right] + s_0(\gamma) \quad (4)$$

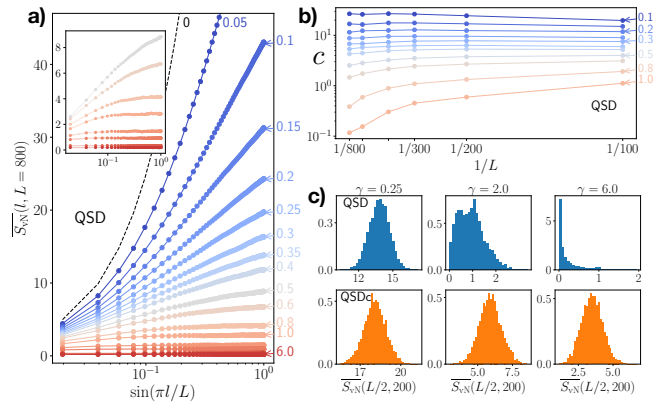


Figure 2. (a) The entanglement entropy as a function of the bipartition size l reveals a clear, asymptotic logarithmic growth for slow monitoring and shows a transition to an area-law for faster monitoring $\gamma \geq \gamma_c$ (inset). (b) Finite size scaling of the central charge c for varying γ (marked) confirms the area law transition at non-zero γ and locates it between $\gamma_c = 0.3$ and $\gamma_c = 0.5$. (c) The trajectory statistics of the entropy reveal a structural difference between the circuit evolution and QSD when the latter is in the area law regime ($L = 200, 5000$ trajectories per histogram).

but with a γ -dependent "central charge" $c(\gamma)$ and residual entropy $s_0(\gamma)$, see Fig. 1(d,e). In thermal equilibrium irrational central charges are unconventional but are found, e.g., in disordered systems [46–48]. However, irrational central charges appear to be characteristic for the critical point of nonequilibrium transitions, including percolation [8, 49] and entanglement transitions both in random circuits and Hamiltonian dynamics [8, 18, 23, 24, 36].

In the QSDc evolution the conformal scaling (4) is observed for any non-zero monitoring and sufficiently large system sizes $L > L_c(\gamma)$. The central charge approaches itself a scaling form $c \sim \gamma^{-\theta}$ with $\theta \approx 0.7$, see Fig. 1(d). This is comparable to an extended conformal invariance in a non-unitary circuit dynamics with disordered free fermions [22], where it was attributed to the spatio-temporal randomness in the combined unitary and non-unitary dynamics. Here, however, we show that the same phenomenon appears when the unitary evolution is disorder free.

A main finding of our work is that this behavior changes qualitatively in the QSD and QJ evolution. For stronger monitoring, e.g., $\gamma \approx 0.4$ for $L = 800$ in Fig. 1(d), the central charge experiences a sudden, strong suppression as a function of γ . For finite system sizes it approaches zero exponentially fast in γ and vanishes above a critical value $\gamma_c(L)$. The transition is evidenced clearly by several different observations (i) a qualitative change in the entanglement entropy, showing no subsystem-dependence for $\gamma \geq 0.6$ in Fig. 2(a), (ii) the scaling of the effective central charge with γ in Fig. 1(d), as well as with the system size L in Fig. 2(b), which drops to zero for $\gamma > 0.5$ and $L \rightarrow \infty$, (iii) the zero-crossing of the residual entropy $s_0(\gamma)$ at $\gamma \approx 0.5$ in Fig. 1(e), which is required for a well-defined, positive entanglement entropy when $c \rightarrow 0$.

and (iv) qualitative changes of the mutual information and the correlation function for $\gamma \geq 0.5$ in Fig. 3.

The precise location of the transition, however, is hard to determine and we estimate $\gamma_c(\infty) \in [0.3, 0.5]$ from the finite size behavior in Fig. 2(b). For stronger monitoring $\gamma \geq \gamma_c$, the entanglement entropy follows an area law $S_{\text{vN}}(l, L) = s_0(\gamma)$, as shown in Fig. 2(a, inset) for $L = 800$. The cutoff approaches the asymptotic value $s_0(\gamma \rightarrow \infty) = 0$. This shows a transition from an extended, supposedly conformally invariant regime to an area law phase for continuously monitored free fermions. Our finding does not contradict earlier work on free fermions, which ruled out a volume law phase at any non-zero monitoring rate but not a subextensive scaling regime [26].

Deviating trajectory ensembles. – All three trajectory evolutions, Eqs. (1), (2) yield qualitatively similar results for small $\gamma \leq \gamma_c$. This includes a subextensive entanglement entropy $\sim \log_2 L$ for large enough system size and an extensive growth for sufficiently small systems. Only the QSD and QJ evolution exhibit, however, a transition towards an area law phase at larger monitoring rates $\gamma \geq \gamma_c$. The QSDc shows no indication of an area law transition and the conformal invariance is extended to arbitrary $\gamma > 0$. This is because for $\gamma \geq \gamma_c$ the nonlinear moments of the correlation matrix start depending significantly on the trajectory evolution and the QSD and QJ evolutions deviate from the QSDc evolution.

This deviation is well illustrated, e.g., by considering the m -th moment of the norm $\mathcal{N}(m) \equiv \langle \psi|\psi \rangle^m$. According to Eqs. (1), (2) one finds (i) $\partial_t \mathcal{N}(m) = 0$ for arbitrary m for the QSD and QJ evolution but (ii) $\partial_t \mathcal{N}(m) \sim \gamma m(m-1)L\mathcal{N}(m)$ for the QSDc evolution [40]. The conservation of all moments $\mathcal{N}(m)$ reveals the exact probability conservation intrinsic to the QSD and QJ evolutions. It is enforced by a stochastic evolution, which evolves the state orthogonally to its Hilbert space location [37, 38]. The QSDc evolution, however, adds a stochastic component parallel to the state, which leads to a different type of trajectories in Hilbert space. This conserves probability only on average, i.e., it conserves exclusively $\mathcal{N}(m=1)$.

We illustrate the difference between QSD and QSDc explicitly by comparing the entanglement entropy distribution for both evolutions in Fig. 2(c). The bins in the histograms reflect the probability for a given entanglement entropy. For weak monitoring, when both types of evolutions predict conformal invariance, both histograms show a distribution with similar mean and variance and which is symmetric around its peak, i.e., both evolutions sample a comparable set of trajectories. The distribution for the QSDc trajectories remains of similar shape for arbitrarily large monitoring rate and only acquires a smaller mean and variance as γ is increased. The distribution of the QSD trajectories, however, undergoes a structural change when it enters the area law phase. It approaches a strongly asymmetric, bimodal distribution with its main peak approaching zero. A second peak emerges and stays pinned at $S_{\text{vN}} = 1$, indicating a pronounced probability for a single non-zero eigenvalue $\lambda = 0.5$ in Eq. (4). In this regime, both distributions deviate structurally from each other, confirming

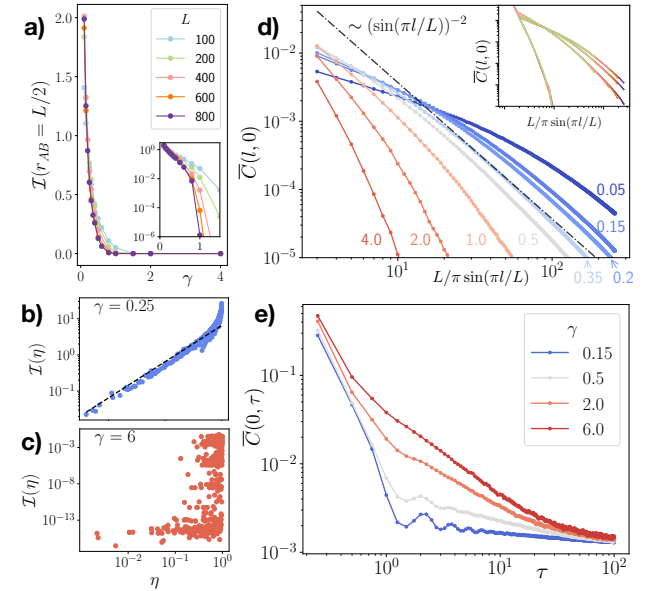


Figure 3. The conformal invariance at weak monitoring is confirmed (a) by a large, non-zero mutual information $l_A = l_B = L/2$, which rapidly decays to zero in the area law regime and (b) by a scaling collapse of the mutual information as a function of the cross ratio η , i.e. $I(\eta) \sim \eta$ ($L=400$). (c) In the area law regime no collapse is observed. (d) Equal time correlations $\bar{C}(l, 0)$ decay algebraically $\sim l^{-2}$ (exponentially) with the distance l in the conformally invariant (area law) regime ($L=800$). The inset shows a data collapse for different system sizes $L = 200, 400, 600, 800$ (axes range identical to main plot) (e) $\bar{C}(0, \tau)$ indicate a quantum-Zeno like evolution with long autocorrelation times in the area law regime ($L=400$).

again that QSD and QSDc yield significantly different dynamics for objects with a nonlinear state dependence.

Mutual information and correlation functions. – In order to verify the extended regime of conformal invariance and an area law transition at non-zero monitoring rate, we investigate several additional indicators, (i) the behavior of the mutual information $I(l_A, l_B)$ between two disjoint intervals A, B, (ii) the equal-time correlation function $\bar{C}(l, 0)$ between two sites at distance l and (iii) the local auto-correlation function $\bar{C}(0, \tau)$.

The mutual information for two disjoint intervals $l_A = l_B = L/8$, with centers at a distance $r_{AB} = L/2$, is expected to show a sharp peak at the critical point separating the area and the volume law phase [18]. Inspecting $I(l_A = l_B = L/8, r_{AB} = L/2)$ for different system sizes in Fig. 3(a) shows that it is significantly larger than zero in the entire critical regime and approaches zero rapidly in the area law phase, reflecting extended criticality. A similar peak is observed for the QJ evolution [40].

For variable subsystem sizes, it is useful to define the cross ratio $\eta = \frac{m_{12}m_{34}}{m_{13}m_{24}}$ with $m_{\alpha\beta} = \sin(\pi|m_\alpha - m_\beta|/L)$. In the conformally invariant regime, the mutual information $I(\eta)$ collapses onto a single line for all η , with a linear increase $\sim \eta$ for small cross ratios. The linear dependence in η also implies a power-law decay of the mutual-information $I \sim r_{AB}^{-2}$ for small subsystems with large separation [18]. This is shown in Fig. 3(b).

This collapse is a strong indication of conformal invariance and can be observed throughout the entire logarithmic regime. It can be contrasted with the behavior in the area law phase, shown in Fig. 3(c), where no collapse is observed.

Also the equal-time correlation functions $\bar{C}(l, 0)$ quantitatively reflect the phase diagram in Fig. 1(b). Their trajectory averages are displayed in Fig. 3(d) for different values of γ . In the conformally invariant regime, i.e., for $0 < \gamma \leq \gamma_c$, two distinct scaling forms are observed depending on whether l is larger or smaller than $L_c(\gamma)$. For $l > L_c(\gamma)$, where the entanglement entropy grows logarithmically, an algebraic decay of the correlation function with the square of the distance $\sim [\sin(\pi l/L)]^{-2}$ is observed. The collapse of the correlation functions for variable system sizes in the inset of Fig. 3(d) demonstrates that this $\sim [\sin(\pi l/L)]^{-2}$ scaling is observed in the thermodynamic limit $L \rightarrow \infty$. On distances $l < L_c(\gamma)$ the correlations decay significantly slower, well approximated by a $\sim l^{-1}$ decay. This can be rationalized with the assumption that the extensive growth reflects an evolution in which sites are entangled up to distances $l \sim L_c(\gamma)$.

When crossing the transition to the area law regime, the correlations start to decay more rapidly with the distance l between different sites. In this regime, a heuristic fit $\bar{C}(l, 0) \sim l^{-5} \exp(-l/l_0)$ yields an increased algebraic decay on short distances compared to the conformally invariant scenario. At larger distances $l > l_0$, the correlations drop to zero exponentially, reflecting short-ranged correlations.

Further information on the dynamics can be inferred from the autocorrelation function $\bar{C}(0, \tau)$. For unitary, free fermions it is easy to show that they are given by the Bessel function $\bar{C}(0, \tau) \sim J_0^2(\tau)$, describing damped oscillations with an envelope decaying as τ^{-1} . While damping of the oscillations increases with γ , the overall decay of the auto-correlations slows down. When entering the area law regime, the oscillations become over-damped and the auto-correlation time is enhanced significantly, indicating a slowly evolving, quantum-Zeno regime, see Fig. 3(e).

Discussion and conclusion. – A natural model of continuously monitored, free fermions can realize an entanglement phase transition if the monitoring protocol preserves probability exactly, which instead of interpolating between volume- and area law behavior, connects a 'gapless' phase with CFT-like logarithmic scaling of the entanglement entropy, to an area law. Beyond exhibiting all of the so far established phenomenology of entanglement transitions, it manifests in the probability distribution of entanglement entropy over trajectories as a new figure of merit.

Our results open up intriguing lines for future research: The simplicity of the model and the phenomenological connections to CFT and the Kosterlitz-Thouless scenario of an extensive critical regime, cut off at a critical dephasing rate γ_c , spark the hope to understand the transition more deeply. Particular attention should be paid to the role played by particle number conservation, which is a prerequisite for gapless behavior even in monitoring-averaged Lindblad dephasing dynamics [50]. Its realizability including the measurement pro-

tocol may play a decisive role in the observability of the established phenomenology.

Acknowledgements. – We acknowledge support from the Deutsche Forschungsgemeinschaft (DFG, German Research Foundation) under Germany's Excellence Strategy Cluster of Excellence Matter and Light for Quantum Computing (ML4Q) EXC 2004/1 390534769, and by the DFG Collaborative Research Center (CRC) 183 Project No. 277101999 - project B02. S.D. and O.A. acknowledge support by the European Research Council (ERC) under the Horizon 2020 research and innovation program, Grant Agreement No. 647434 (DOQS). M.B. acknowledges funding via grant DI 1745/2-1 under DFG SPP 1929 GiRyd. The code for our numerical computations was written in Julia [51]. We furthermore thank the Regional Computing Center of the University of Cologne (RRZK) for providing computing time on the DFG-funded High Performance Computing (HPC) system CHEOPS as well as support.

Numerical implementation

Here, we provide details for the numerical implementation of the trajectory evolution described in the main text, Eqs. (1), (2). For each individual trajectory, the state at time t is a Gaussian state, which is parametrized by an $L \times N$ matrix $U(t)$ with elements $u_{ij}(t)$. It satisfies $U^\dagger U = \mathbb{1}$.

To simulate the quantum state diffusion we follow the Trotterization approach used in Ref. [26]. Evolving U over time step dt and neglecting corrections of order $(dt)^2$ yields up to an overall normalization

$$U(t + dt) = \text{diag}(e^{\xi_{1,t} + \gamma\sigma(2\langle n_1 \rangle_t - 1)dt}, \dots, e^{\xi_{N,t} + \gamma\sigma(2\langle n_N \rangle_t - 1)dt}) e^{-ihdt} U,$$

where h is the hopping matrix, $\sigma = 1$ (QSD) or $\sigma = 0$ (QSDc) and the $\langle n_i \rangle_t$ are computed from the correlation matrix $D_{l,l}(t, t)$. We then ensure that the columns of U are orthonormal by performing a QR decomposition $U = QR$ and redefining $U = Q$. The applied step size is $dt = 0.05$.

To simulate the quantum-jump evolution Eq. (2), we exploit that particle number conservation enforces a constant jump rate γN and apply the common jump evolution procedure described [39]. (i) Determine the jump time $\tau = -\log(r)/(\gamma N)$ by drawing a random number r uniformly from $[0, 1]$. (ii) Evolve the time step t to $t + \tau$ via $U(t + \tau) = e^{-i\hbar\tau} U(t)$ and choose a jump operator n_j according to the probabilities $P(n_j) = \langle n_j \rangle_{t+\tau}/N$. (iii) Apply the jump to the correlation matrix $D = U(t + \tau)U^\dagger(t + \tau)$ according to

$$D_{lm} \rightarrow \begin{cases} 1, & l = m = j \\ 0, & l \neq m \text{ and } (l = j \text{ or } m = j) \\ D_{lm} - \frac{D_{jm}D_{lj}}{\langle n_j \rangle_t}, & \text{otherwise} \end{cases}.$$

(iv) Obtain the new U matrix by performing an SVD decomposition $D = USU^\dagger$ for a hermitian matrix D (note $S_{11} = \dots = S_{NN} = 1, S_{N+1,N+1} = \dots = S_{LL} = 0$).

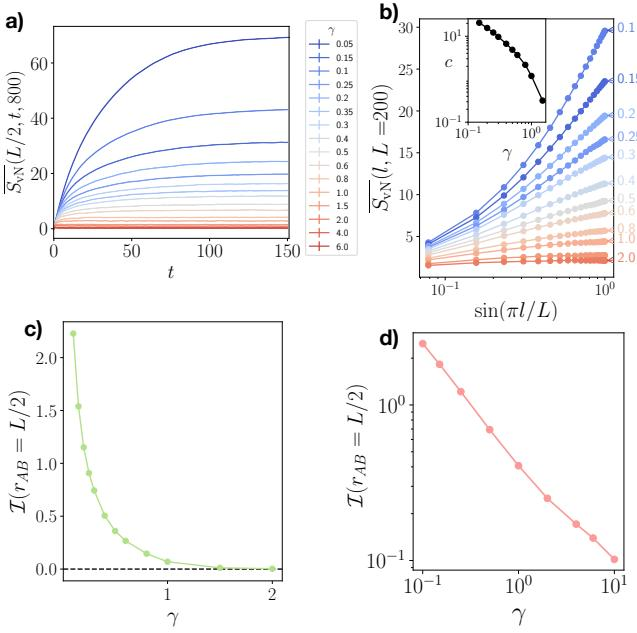


Figure 4. (a) Time dependence of the trajectory average entanglement-entropy for an equal bi-partition of a system of size $L = 800$, in the QSD evolution. (b,c) Observables for the QJ evolution (Eq. (2)) for $L = 200$. (b) The entanglement entropy as a function of the subsystem size l for different monitoring rates (marked on the figure). The inset shows the effective central charge as a function of γ . (c) The mutual-information of two subsystems with lengths $l_A = l_B = L/8$, with distance $r_{AB} = L/2$ between their centers. (d) Mutual information of two subsystems with lengths $l_A = l_B = L/8$ and relative distance $r_{AB} = L/2$ from the QSDc evolution for $L = 400$. The mutual information \mathcal{I} exhibits a power-law decay with increasing γ over the full parameter range and never drops to zero as sharply as in QSD or QJ.

Quantum jump results

Here we provide results for the QJ evolution, which are discussed in the main text but not displayed in the figures for clarity. The entanglement entropy, Fig. 4(a), and the mutual information, Fig. 4(b), in the QJ evolution are qualitatively comparable to the entanglement entropy obtained from QSD in Fig. 2(a). Both confirm an extended critical regime where $\mathcal{I}_{A,B}(r_{AB} = L/2)$ is non-zero and the entanglement entropy grows logarithmically with system size for weak monitoring ($\gamma \leq 1$ for $L = 200$). At stronger monitoring, both observables indicate an area-law regime where the mutual-information drops to zero. In general we observe that the boundary between critical and area-law behavior seems to be shifted to larger γ for the QJ evolution for any system size L . However, this contrasts clearly the absence of an area law phase in the QSDc evolution, as indicated by the non-vanishing mutual information in Fig. 4 (d).

Higher moment evolution

Observables, which depend on higher moments of the state $|\psi_t\rangle\langle\psi_t|$ may strongly depend on the specific trajectory evolution. An example is the entanglement entropy in the main text. Here we illustrate this with a simple analytical example, the m -th moment of the norm $\langle\psi_t|\psi_t\rangle^m$. We start with the QSD evolution (1) and, for simplicity, a single, hermitian Lindblad operator \hat{M} . The scaling $\xi_t \sim \sqrt{dt}$ requires that infinitesimal changes are taken into account up to order d^2 . Up to this order, the infinitesimal change is

$$d\langle\psi_t|\psi_t\rangle^m = m\langle\psi_t|\psi_t\rangle^{m-1}(\langle\psi_t|d\psi_t\rangle + \langle d\psi_t|\psi_t\rangle + \langle d\psi_t|d\psi_t\rangle) + m(m-1)\langle\psi_t|\psi_t\rangle^{m-2}(\langle d\psi_t|\psi_t\rangle + \langle\psi_t|d\psi_t\rangle)^2. \quad (5)$$

The Hamiltonian evolution cancels out and expanding again up to order dt one finds

$$d\langle\psi_t|\psi_t\rangle^m = m\langle\psi_t|\psi_t\rangle^{m-1}[(\xi^2 - \gamma dt)\langle\psi_t|\hat{M}^2|\psi_t\rangle + \xi\langle\psi_t|\hat{M}|\psi_t\rangle] + 2m(m-1)\langle\psi_t|\psi_t\rangle^{m-2}\xi^2\langle\psi_t|\hat{M}|\psi_t\rangle^2. \quad (6)$$

The trajectory average thus yields

$$\overline{d\langle\psi_t|\psi_t\rangle^m} = 2\gamma m(m-1)\overline{\langle\psi_t|\psi_t\rangle^m\langle\hat{M}\rangle_t^2}dt, \quad (7)$$

where $\langle\hat{M}\rangle_t = \langle\psi_t|\hat{M}|\psi_t\rangle/\langle\psi_t|\psi_t\rangle$. For the first moment, $m = 1$, the term on the right always vanishes, enforcing that the trajectory averaged norm is constant. Higher moments, however, do generally not vanish and their evolution depends on the operator \hat{M} . For QSDc, $\hat{M} = n$ is the particle number operator, and one observes in general an exponential growth of the higher moments with an approximate rate $2\gamma m(m-1)\langle n \rangle^2$. For QSD, however, $\hat{M} = n - \langle n \rangle$, such that $\langle\hat{M}\rangle_t = 0$ for any state and thus any moment m of the norm remains constant over time.

The norms in the QJ evolution are more involved because here $\xi^2 = \xi \sim dt$ and thus arbitrarily high powers in ξ contribute to the evolution of $\langle\psi_t|\psi_t\rangle^m$. We restrict ourselves to $m = 1, 2$ and again use the operator shortcut $\hat{M} = \left(\frac{n}{\sqrt{\langle n \rangle}} - 1\right)$. This yields

$$d\langle\psi_t|\psi_t\rangle = \xi\langle\psi_t|\hat{M}^2 + 2\hat{M}|\psi_t\rangle = 0, \quad (8)$$

$$d\langle\psi_t|\psi_t\rangle^2 = \xi\langle\psi_t|\psi_t\rangle[\langle\hat{M}\rangle^2 + 4\langle\hat{M}\rangle\langle\hat{M}^2\rangle + \langle\hat{M}^2\rangle^2] = 0. \quad (9)$$

Here, only the property $\xi^2 = \xi$ was exploited and no trajectory average was required to show that the evolution is constant for this type of jump operator.

This example can be easily generalized to multiple jump operators \hat{M} and demonstrates that in QSD and QJ trajectories all higher moments of the norm remain constant over time up to order dt^2 and an initially normalized state remains normalized. For QSDc on the other hand, higher moments $m > 1$ grow roughly exponentially in time, demonstrating that only the average norm of the state is conserved while its variance is blowing up.

We emphasize that the difference between the different trajectory evolutions is not just a matter of normalization: the additional parallel evolution in QSDc yields trajectories, which

explore are different Hilbert space than the trajectories from QSD and QJ. This difference is not resolved by an adhoc normalization of the state after each numerical time step [37].

[1] B. R. Mollow, *Phys. Rev. A* **12**, 1919 (1975).

[2] R. H. Dicke, *American Journal of Physics* **49**, 925 (1981), <https://doi.org/10.1119/1.12592>.

[3] D. Leibfried, R. Blatt, C. Monroe, and D. Wineland, *Rev. Mod. Phys.* **75**, 281 (2003).

[4] V. N. Golovach, A. Khaetskii, and D. Loss, *Phys. Rev. Lett.* **93**, 016601 (2004).

[5] D. D. Sukachev, A. Sipahigil, C. T. Nguyen, M. K. Bhaskar, R. E. Evans, F. Jelezko, and M. D. Lukin, *Phys. Rev. Lett.* **119**, 223602 (2017).

[6] Results represent averages over 500 trajectories for $L \leq 600$ and 300 trajectories for $L = 800$.

[7] A. Nahum, J. Ruhman, S. Vijay, and J. Haah, *Phys. Rev. X* **7**, 031016 (2017).

[8] B. Skinner, J. Ruhman, and A. Nahum, *Phys. Rev. X* **9**, 031009 (2019).

[9] Y. Li, X. Chen, and M. P. A. Fisher, *Phys. Rev. B* **98**, 205136 (2018).

[10] A. Chan, R. M. Nandkishore, M. Pretko, and G. Smith, *Phys. Rev. B* **99**, 224307 (2019).

[11] S. Choi, Y. Bao, X.-L. Qi, and E. Altman, “Quantum error correction in scrambling dynamics and measurement induced phase transition,” (2019), [arXiv:1903.05124 \[quant-ph\]](arXiv:1903.05124).

[12] C.-M. Jian, Y.-Z. You, R. Vasseur, and A. W. W. Ludwig, *Phys. Rev. B* **101**, 104302 (2020).

[13] M. J. Gullans and D. A. Huse, “Dynamical purification phase transitions induced by quantum measurements,” (2019), [arXiv:1905.05195 \[quant-ph\]](arXiv:1905.05195).

[14] A. Zabalo, M. J. Gullans, J. H. Wilson, S. Gopalakrishnan, D. A. Huse, and J. H. Pixley, *Phys. Rev. B* **101**, 060301 (2020).

[15] L. Zhang, J. A. Reyes, S. Kourtis, C. Chamon, E. R. Mucciolo, and A. E. Ruckenstein, “Nonuniversal entanglement level statistics in projection-driven quantum circuits,” (2020), [arXiv:2001.11428 \[cond-mat.stat-mech\]](arXiv:2001.11428).

[16] Q. Tang and W. Zhu, *Phys. Rev. Research* **2**, 013022 (2020).

[17] Y. Bao, S. Choi, and E. Altman, *Physical Review B* **101** (2020), 10.1103/physrevb.101.104301.

[18] Y. Li, X. Chen, and M. P. A. Fisher, *Physical Review B* **100**, 134306 (2019), <arXiv:1901.08092>.

[19] M. J. Gullans and D. A. Huse, “Scalable probes of measurement-induced criticality,” (2019), [arXiv:1910.00020 \[cond-mat.stat-mech\]](arXiv:1910.00020).

[20] M. Szyniszewski, A. Romito, and H. Schomerus, *Phys. Rev. B* **100**, 064204 (2019).

[21] S. Goto and I. Danshita, “Measurement-induced transitions of the entanglement scaling law in ultracold gases with controllable dissipation,” (2020), [arXiv:2001.03400 \[cond-mat.quant-gas\]](arXiv:2001.03400).

[22] Y. Li, X. Chen, A. W. W. Ludwig, and M. P. A. Fisher, “Conformal invariance and quantum non-locality in hybrid quantum circuits,” (2020), [arXiv:2003.12721 \[quant-ph\]](arXiv:2003.12721).

[23] Y. Fuji and Y. Ashida, “Measurement-induced quantum criticality under continuous monitoring,” (2020), [arXiv:2004.11957 \[cond-mat.stat-mech\]](arXiv:2004.11957).

[24] X. Chen, Y. Li, M. P. A. Fisher, and A. Lucas, “Emergent conformal symmetry in non-unitary random dynamics of free fermions,” (2020), [arXiv:2004.09577 \[quant-ph\]](arXiv:2004.09577).

[25] H. Pichler, J. Schachenmayer, A. J. Daley, and P. Zoller, *Physical Review A* **87** (2013), 10.1103/physreva.87.033606.

[26] X. Cao, A. Tilloy, and A. De Luca, *SciPost Physics* **7** (2019), 10.21468/scipostphys.7.2.024.

[27] D. Poletti, J.-S. Bernier, A. Georges, and C. Kollath, *Phys. Rev. Lett.* **109**, 045302 (2012).

[28] M. Knap, *Phys. Rev. B* **98**, 184416 (2018).

[29] S. Sarkar, S. Langer, J. Schachenmayer, and A. J. Daley, *Physical Review A* **90** (2014), 10.1103/physreva.90.023618.

[30] S. de Léséleuc, D. Barredo, V. Lienhard, A. Browaeys, and T. Lahaye, *Phys. Rev. A* **97**, 053803 (2018).

[31] S. Helmrich, A. Arias, and S. Whitlock, *Phys. Rev. A* **98**, 022109 (2018).

[32] D. Yang, C. Laflamme, D. V. Vasilyev, M. A. Baranov, and P. Zoller, *Phys. Rev. Lett.* **120**, 133601 (2018).

[33] I. de Vega and D. Alonso, *Rev. Mod. Phys.* **89**, 015001 (2017).

[34] H. M. Wiseman and G. J. Milburn, *Phys. Rev. A* **47**, 1652 (1993).

[35] J. Dalibard, Y. Castin, and K. Mølmer, *Phys. Rev. Lett.* **68**, 580 (1992).

[36] M. Ippoliti, M. J. Gullans, S. Gopalakrishnan, D. A. Huse, and V. Khemani, “Entanglement phase transitions in measurement-only dynamics,” (2020), [arXiv:2004.09560 \[quant-ph\]](arXiv:2004.09560).

[37] N. Gisin and I. C. Percival, *Journal of Physics A: Mathematical and General* **25**, 5677 (1992).

[38] L. Diósi, N. Gisin, and W. T. Strunz, *Phys. Rev. A* **58**, 1699 (1998).

[39] A. J. Daley, *Advances in Physics* **63**, 77149 (2014).

[40] See supplementary material appended to this manuscript.

[41] P. Calabrese and J. Cardy, *Journal of Statistical Mechanics: Theory and Experiment* **2005**, P04010 (2005).

[42] V. Alba and P. Calabrese, *SciPost Phys.* **4**, 17 (2018).

[43] This dependence was estimated by solving $\frac{c(\gamma)}{3} \log_2(L_c(\gamma)/\pi) + s(\gamma) = 0$ with the scaling behavior for $s(\gamma)$, $c(\gamma)$ from the simulations.

[44] P. Calabrese and J. Cardy, *Journal of Statistical Mechanics: Theory and Experiment* **2004**, P06002 (2004).

[45] P. Calabrese and J. Cardy, *Journal of Physics A: Mathematical and Theoretical* **42**, 504005 (2009).

[46] J. Cardy and J. L. Jacobsen, *Phys. Rev. Lett.* **79**, 4063 (1997).

[47] G. Refael and J. E. Moore, *Physical Review Letters* **93** (2004), 10.1103/physrevlett.93.260602.

[48] N. Laflorencie, *Phys. Rev. B* **72**, 140408 (2005).

[49] J. Cardy, *Phys. Rev. Lett.* **84**, 3507 (2000).

[50] Z. Cai and T. Barthel, *Phys. Rev. Lett.* **111**, 150403 (2013).

[51] J. Bezanson, A. Edelman, S. Karpinski, and V. B. Shah, *SIAM review* **59**, 65 (2017).